This article has been accepted for publication in a future issue of this journal, but has not been fully edited. Content may change prior to final publication. Citation information: DOI 10.1109/TSG.2018.2822276, IEEE Transactions on Smart Grid

Optimal Management of Energy Consumption and Comfort for Smart Buildings Operating in a Microgrid

Jerson A. Pinzon, Pedro P. Vergara, Luiz C. P. da Silva, and Marcos J. Rider, *Senior Member, IEEE*

***Abstract*—This paper presents a mixed integer non-linear programming (MINLP) model to optimize, in a centralized fashion, the operation of multiple buildings in a microgrid. The proposed model aims to minimize the total cost of the energy imported from the main grid at the interconnection point, managing the power demand and generation of buildings, while operational constraints of the electrical grid are guaranteed. This approach considers the management of heating, ventilation and air conditioning (HVAC) units, lighting appliances, photovoltaic generation (PV) and energy storage system (ESS) of each building. Comfortable indoor conditions for the occupants are kept by a set of mathematical constraints. Additionally, a strategy that simplifies the original model is presented, based on a set of linearization techniques and equivalent representations, obtained through a pre-processing stage executed in EnergyPlus software. This strategy allows approximating the proposed model into a mixed integer linear programming (MILP) formulation that can be solved using commercial solvers. The proposed model was tested in a 13-bus microgrid for different deterministic cases of study with non-manageable loads and smart buildings. A large-size test case is also considered. Finally, a rolling horizon (RH) strategy is proposed with the aim of addressing the uncertainty of the data, as well as reducing the amount of forecasting data required.**

***Index Terms*—Smart buildings, microgrid, linear programming, energy and comfort management, optimization.**

I. Notation

Sets and Indexes:

$\mathcal{T}$	Set of time steps
$\mathcal{N}$	Set of buses
$\mathcal{L}$	Set of branches
$\mathcal{Z}_i$	Set of zones of the building i
$\mathcal{T}^{\kappa}_{i,z}$	Set of occupied time steps of the zone z in building i
z	Zone $z \in \mathcal{Z}_i$
t	Time interval $t \in \mathcal{T}$
i	Bus $i \in \mathcal{B}$
ij	Branch $ij \in \mathcal{L}$
λ	λth block used for the piecewise linearization

Parameters:

α_t	Energy price, [$/kWh]
A^{PV}_i	Area of the PV array, [m^2]
$\underline{C}_i$	Minimum permissible comfort index
c^{Air}, ρ^{Air}	Specific heat and density of the air
$COP_{i,z}$	Coefficient of performance of HVAC unit
Δt	Duration of the time step
$\overline{\delta}^{I}_{i,z}$, $\overline{\delta}^{T}_{i,z}$	Discretization steps of the piecewise linearization of $\Delta^{I}_{i,z,t}$, $\Delta^{T}_{i,z,t}$
$\overline{\delta}^{P}_{ij}$, $\overline{\delta}^{Q}_{ij}$	Discretization steps of the piecewise linearization of $P_{ij,t}$, $Q_{ij,t}$
$\delta^{T_{Fan}}$	Fan rise in air temperature, [^{o}C]
$\delta^{Srf}_{i,z,t}$	Heat increment used to define $q^{Srf}_{i,z,t}$
E^{N}_i	Nominal energy of the ESS, [kWh]
$\overline{E}^{B}_i$	Maximum charging/discharging energy of the ESS, [kWh]
η^{CH}_i, η^{DH}_i	Efficiency of ESS system
η^{PV}_i	Efficiency of PV system
$\eta^{Fan}_{i,z}$	Efficiency of the fan motor
fp_i	Building power factor
$\zeta_{i,z}$	Lighting especial allowance factor
G_t	Irradiance, [W/m^2]
$\overline{\gamma}_i$	Maximum charge/discharge cycles of the ESS
h^{Ed}, h^{Oc}	Electrical devices and people single heat gain
$\kappa^{Oc}_{i,z,t}$, $\kappa^{Ed}_{i,z,t}$	Electrical devices usage and occupancy profiles
β, T_{STC}	Design parameters of the PV array
$I^{o}_{i,z,t}$, $T^{o}_{i,z,t}$	Set points during the pre-processing stage
$I^{N}_{i,z,t}$	External/natural illuminance component
$LP_{i,z}$	Lighting power ratio, [W/Lx]
$\sigma^{I}_{i,z,y}$, $\sigma^{T}_{i,z,y}$	Slope of the λth block used for the piecewise linearization of $\Delta^{I}_{i,z,t}$, $\Delta^{T}_{i,z,t}$
$\sigma^{P}_{ij,y}$, $\sigma^{Q}_{ij,y}$	Slope of the λth block used for the piecewise linearization of $P_{ij,t}$, $Q_{ij,t}$
ψ', ψ''	Parameters for linear regression of $f^{SHR}_{i,z,t}$
$\mu o^{I}_{i,z}$	Illuminance comfortable set point, [Lx]
$\underline{\mu o}^{I}_{i,z}$, $\overline{\mu o}^{I}_{i,z}$	Minimum and maximum illuminance, [Lx]
$\mu o^{T}_{i,z}$	Temperature comfortable set point, [^{o}C]
$\underline{\mu o}^{T}_{i,z}$, $\overline{\mu o}^{T}_{i,z}$	Minimum and maximum temperature, [^{o}C]
$P^{Fan}_{i,z}$	Fan power, [W]
$P^{PV}_{i,t}$	Active power supplied by the PV system, [kW]
$P^{BL}_{i,t}$	Non-manageable demand of buildings, [kW]
$\underline{P}^{HVAC}_{i,z}$, $\overline{P}^{HVAC}_{i,z}$	Minimum and maximum power of HVAC unit
$q^{N}_{i,z}$	Rated total cooling capacity of HVAC unit, [W]
$q^{Ed}_{i,z,t}$, $q^{Oc}_{i,z,t}$	Electrical devices and people heat gain, [W]

This work was supported by the Sao Paulo Research Foundation (FAPESP). Research grants: 2015/18145-0 and 2015/09136-8.

Jerson A. Pinzon, Pedro. P. Vergara, Luiz C. P. da Silva and Marcos J. Rider are with the Department of Systems and Energy, UNICAMP–University of Campinas, Campinas, São Paulo, 13083-852, Brazil, emails:{jpinzon, pedropa, lui, mjrider}@dsee.fee.unicamp.br

This article has been accepted for publication in a future issue of this journal, but has not been fully edited. Content may change prior to final publication. Citation information: DOI 10.1109/TSG.2018.2822276, IEEE Transactions on Smart Grid

$q_{i,z,t}^{Srfo}$	Surfaces heat gain in pre-processing stage, W
$q_{i,z,t}^{Loss}$	Thermal fan losses, [W]
R_{ij}, X_{ij}	Resistance and reactance of the branch ij
$F_{i,z}^{SHR}$	Nominal sensible heat ratio
$\underline{SOC}_i$, $\overline{SOC}_i$	Minimum and maximum SOC of the ESS
SOC^F	SOC at the end of the horizon
$v_{i,z}$	Zone volume, [m^3]
$\tau\kappa_{i,z}^{Oc}$	Total period of occupancy per zone
T_t^{Out}	Outside temperature, [^{o}C]
$\nu_{i,z}^{Inf}$, $\nu_{i,z}^{Fan}$	Infiltration and ventilation flow rate, [m^3/s]
$\underline{V}$, $\overline{V}$	Minimum and maximum voltage thresholds
$V_{i,t}^{'}$	Estimated value of the voltage magnitude
ω_i^I, ω_i^T	Weight factors of visual and thermal comfort
$\overline{\lambda}$	Number of blocks for the piecewise formulation
Z_{ij}	Impedance of the branch ij

Continuous Variables:

$C_{i,z}$	Global comfort index
$C_{i,z,t}^I$, $C_{i,z,t}^T$	Visual and thermal comfort factors
$\Delta_{i,z,t}^I$, $\Delta_{i,z,t}^T$	Deviations from comfortable set points
$E_{i,t}^{CH}$, $E_{i,t}^{DCH}$	Charging/discharging energy of the ESS, [kWh]
$E_{i,z,t}^I$, $E_{i,z,t}^T$	Energy of lighting and HVAC appliances, [Wh]
$F_{i,z,t}^{EIR}$	Energy input ratio of HVAC unit
$f_{i,z,t}^{CCT}$, $f_{i,z,t}^{CCF}$	Cooling capacity modifier factors
$f_{i,z,t}^{EIT}$, $f_{i,z,t}^{EIF}$	Energy input ratio modifier factors
$f_{i,z,t}^{SHR}$	Sensible heat ratio modifier factor
$I_{i,z,t}$	Zone illuminance set point, [Lx]
$I_{i,j,t}^{sqr}$	Squared of current through branch i,j
$F_{i,z,t}^{PLR}$	Part load ratio of HVAC unit
$P_{ij,t}$, $Q_{ij,t}$	Active and reactive power flow of branch ij
$P_{i,t}^{BD}$, $Q_{i,t}^{BD}$	Active and reactive internal power balance of building i
$P_{i,t}^L$, $Q_{i,t}^L$	Active and reactive power demand of non-manageable load i
$q_{i,z,t}^{Inf}$, $q_{i,z,t}^{Ven}$	Infiltration and ventilation heat gain, [W]
$q_{i,z,t}^L$	Lighting appliances heat gain, [W]
$q_{i,z,t}^{Srf}$	Surfaces heat gain, [W]
$q_{i,z,t}^{Sto}$	Heat stored in the zone air volume, [W]
$q_{i,z,t}^S$	Sensible cooling load of the zone, [W]
$q_{i,z,t}^T$	Total cooling capacity of the cooling coil, [W]
$F_{i,z,t}^{RTF}$	Run time fraction of HVAC unit
$\Phi_{i,t}^T$	Variable used to represent $(T_{i,z,t} \cdot u_{i,z,t})$
$\Gamma_{i,t}^{CH}$, $\Gamma_{i,t}^{DH}$	Variables used to represent $(b_{i,t}^{CH} \cdot b_{i,t-1}^{CH})$ and $(b_{i,t}^{DH} \cdot b_{i,t-1}^{DH})$
$SOC_{i,t}$	State of charge
$T_{i,z,t}$	Zone temperature set point, [^{o}C]
$V_{i,t}^{sqr}$	Squared of voltage at bus i

Binary Variables:

$u_{i,z,t}$	Variable of the operation of HVAC unit
$b_{i,t}^{CH}$, $b_{i,t}^{DH}$	Variables associated with the charging/discharging mode of the ESS

II. Introduction

BUILDINGS consume about 32% of the total electrical energy and are responsible for approximately 30% of CO_2 emissions worldwide [1]. This fact has promoted the development of building energy management systems (BEMS), which integrate distributed generation (DG), demand response (DR) schemes and management of occupants' comfort, aiming to reduce energy consumption [2], [3]. Additionally, if the BEMS operation is coordinated with the electrical grid, events such as insufficient renewable-based generation, energy price fluctuations, voltage limits violations, among others, can be mitigated [4], [5].

In the literature, three modeling approaches have been used to represent building operation: data-driven models [6], thermal resistance-capacitance (RC) representations [7], [8], and high fidelity physical formulations [9]–[12]. Data-driven models are based on large historical data, they provide good performance operating with the trained data set. However, the inaccuracy of these models can increase when events outside the trained set occur. As for RC models, they are used to represent a simplified form of physical phenomena, providing an accurate prediction of important thermal states of buildings [7]. Nevertheless, estimating the parameters of these models requires complex characterization procedures [13]. Finally, high fidelity physical models capture accurate thermal interactions of buildings by using complex formulations. For instance, in [9], a detailed model to describe the thermal dynamics of a building is presented. The interaction between the building and different energy storage technologies is studied. In [10], a mixed integer linear programming (MILP) model is used to manage electrical and thermal resources aiming to minimize the total cost in a house, coordinating the operation of photovoltaic system (PV), energy storage system (ESS), combined heat and power (CHP) unit and thermal storage. In [11], a co-simulation strategy executes an iterative method to find the optimal operation of heating, ventilation and air-conditioning (HVAC) units, PV and ESS, simulating a candidate solution in EnergyPlus at each iteration. A similar approach is presented in [12]. Nevertheless, the main disadvantages of these models are related to their size and complexity, requiring a large processing time. Thus, these formulations cannot be easily incorporated into on-line optimization schemes, which are responsible for the energy management decisions [7].

Regarding the interaction between buildings and the electrical grid, in [14] the integration of building loads, DGs and distribution grid is studied through a market approach. In [15], the impact of the operation of a building on the grid is evaluated using indicators such as loss-of-load probability, and a cover factor for supply and demand. Nevertheless, in these works, little attention is given to the electrical grid operation. On the other hand, authors in [16] include the modeling of the distribution grid, but disregards PV and ESS operation, as well as appliances such as the lighting system, which is considered one of the largest loads and depending on the technology[1], it may represent a big share of the space heat gain [19].

[1]For instance, fluorescent appliances turn about 80% of their power consumption into heat [17], and LED appliances near to 75% [18].

This article has been accepted for publication in a future issue of this journal, but has not been fully edited. Content may change prior to final publication. Citation information: DOI 10.1109/TSG.2018.2822276, IEEE Transactions on Smart Grid

In order to address this, a mixed integer non-linear programming (MINLP) model is presented in this paper to optimize, in a centralized fashion, the operation of multiple buildings in a microgrid. From the microgrid's operator point of view, the proposed model aims to minimize the total cost of the energy traded at the interconnection point with the main grid, while operational constraints of the electrical grid are guaranteed. This approach is based on a high fidelity physical model which considers the management of HVAC units, lighting appliances, PV and ESS of each building. Comfortable indoor conditions for the occupants are kept by a set of mathematical constraints. Additionally, a strategy that simplifies the original model is presented, based on a set of linearization techniques and equivalent representations, obtained through a pre-processing stage executed in EnergyPlus [20]. This strategy allows approximating the proposed model into an MILP formulation, that can be solved using commercial solvers. The proposed model was tested in a 13-bus microgrid, which may represent a cluster of buildings in a campus university or military facilities.

Regarding uncertainty in the data, a rolling horizon (RH) scheme is also proposed in this paper. This RH scheme allows reducing the amount of forecasting data required. In general, strategies to address uncertainty in scheduling problems can be classified in two main groups [21], named as proactive and reactive strategies. Proactive approaches are based on the consideration of all possible cases, mainly based on stochastic programming theory. For instance, in [22], it is presented a stochastic model for building operation that takes into account the uncertainty of weather predictions; in [23], authors present a distributed approach based on a locational marginal price method for buildings in distribution grids, considering uncertainties through a stochastic disturbance. However, the solution of proactive strategies may be too conservative, since the model takes into account all the possible scenarios of the stochastic variables, including the ones that eventually does not occur [21]. On the other hand, reactive approaches aim at modifying a predefined schedule, in order to adjust it to disturbances or updated system data. Rolling horizon schemes belong to this category. For instance, in [24], an MILP based rolling optimization approach under real time pricing policy is introduced to manage energy consumption of a smart home; in [25], an energy management system based in a RH strategy for a renewable-based microgrid is proposed.

Compared with a preliminary version of this work presented in [26], this paper provides extensions in the form of (*i*) optimization of the operation of multiple buildings, (*ii*) inclusion of the operation and technical constraints of the electrical grid and (*iii*) consideration of the uncertainty in forecasting data. Thus, the main contributions of this paper can be summarized as follows:

- An MINLP model, which describes the operation of multiple buildings in conjunction with the microgrid, considering the management of the energy and comfort in buildings and technical constraints of the electrical grid;
- A solution strategy that simplifies the original model using an MILP formulation in conjunction with a pre-processing stage executed in EnergyPlus. This strategy reduces the complexity of the optimization problem, allowing the use of convex commercial solvers that guarantee optimality.

III. Proposed MINLP Model

The proposed MINLP model describes the operation of multiple buildings in a microgrid at the distribution level. It is considered that each building has a BEMS to manage the energy consumption through controlling HVAC units and lighting appliances across the set of zones $\mathcal{Z}_i$. Also, it is assumed that buildings are equipped with a PV and an ESS, comprised by battery banks. The microgrid's operator minimizes the total cost of the energy traded at the interconnection point with the main grid as in (1),

$$\min \quad \left\{ \sum_{t\in\mathcal{T}} \alpha_t \left[\sum_{i\in\mathcal{N}} P^{BD}_{i,t} \Delta t + \sum_{ij\in\mathcal{L}} R_{ij} I^2_{ij,t} \Delta t \right] \right\} \tag{1}$$

Here the first term refers to the buildings internal energy balance (which can be negative if local generation is greater than consumption), while the second term refers to the active power losses in the grid. Notice in (1) that aggregated loads ($P^L_{i,t}$) are not considered since they are non-manageable. The optimal operation (i. e., decision variables) is defined by the schedule of ESS charging/discharging profile ($E^{CH}_{i,t}, E^{DH}_{i,t}$), and temperature ($T_{i,z,t}$) and illuminance ($I_{i,z,t}$) set points in the zones of all the buildings, as well as the operational state of HVAC units ($u_{i,z,t}$).

A. Electrical Grid Model

The electrical grid is represented by the balanced non-linear power flow equations defined by (2)–(7). This model is suitable since buildings usually operate at medium voltage distribution level due to their large energy consumption. Equations (2) and (3) model the active and reactive power balance, respectively. Here, $P^L_{i,t}, Q^L_{i,t}$ represent the active and reactive non-manageable loads, meanwhile $P^{BD}_{i,t}, Q^{BD}_{i,t}$ model the active and reactive internal power balance of buildings[2] (see Sec. III-B). The voltage drop in lines is defined by (4), while the definition of current magnitude through lines is describe by (5). Finally, constraints (6) and (7) define the voltage and current magnitude limits, respectively.

$$\sum_{ji\in\mathcal{L}} P_{ji,t} - \sum_{ij\in\mathcal{L}} \left(P_{ij,t} + R_{ij} I^2_{ij,t}\right) = P^{BD}_{i,t} + P^L_{i,t} \quad \forall ij,t \tag{2}$$

$$\sum_{ji\in\mathcal{L}} Q_{ji,t} - \sum_{ij\in\mathcal{L}} \left(Q_{ij,t} + X_{ij} I^2_{ij,t}\right) = Q^{BD}_{i,t} + Q^L_{i,t} \quad \forall ij,t \tag{3}$$

$$V^2_{i,t} - V^2_{j,t} = 2\left(R_{ij}P_{ij,t} + X_{ij}Q_{ij,t}\right) - Z^2_{ij} I^2_{ij,t} \quad \forall ij,t \tag{4}$$

$$V^2_{i,t} I^2_{ij,t} = P^2_{ij,t} + Q^2_{ij,t} \quad \forall ij,t \tag{5}$$

$$\underline{V} \le V_{i,t} \le \overline{V} \quad \forall i,t \tag{6}$$

$$I_{ij,t} \le \overline{I}_{ij} \quad \forall ij,t \tag{7}$$

[2]Henceforth, it is assumed that building *i* is connected to the bus $i \in \mathcal{N}$. Additionally, if there is no building or load at bus *i*, then $P^{BD}_{i,t} = Q^{BD}_{i,t} = 0$ and $P^L_{i,t} = Q^L_{i,t} = 0$.

This article has been accepted for publication in a future issue of this journal, but has not been fully edited. Content may change prior to final publication. Citation information: DOI 10.1109/TSG.2018.2822776, IEEE Transactions on Smart Grid

B. Internal Power Balance of Buildings

The internal power balance of each building is defined by (8), as function of the non-manageable internal demand ($P_{i,t}^{BL}$), the HVAC units and lighting system consumption ($E_{i,z,t}^{T}$ and $E_{i,z,t}^{I}$, respectively), generation of PV ($P_{i,t}^{PV}$), and ESS charging/discharging energy ($E_{i,t}^{DC}$ and $E_{i,t}^{DH}$). The reactive power demand in (9) depends on the active power consumption and the power factor (fp_i), which is considered to be constant. PV generation is modeled as in (10), based on forecasted irradiance (G_t) and temperature (T_t^{OUT}) information. The ESS is modeled using (11)–(18), based on [27]. The state of charge is defined as in (11). Charging/discharging states are defined through the binary variables $b_{n,t}^{CH}$, $b_{n,t}^{DH}$ in (12)–(13). Here, $\overline{E}_i^B$ limits the amount of energy during the charging and discharging operation, aiming to reduce the effects over the state-of-health of the ESS. Constraint (14) is used to model the unimodality operation of the ESS, i. e., the requirement to operate in only one state (charging, discharging or stand-by). Additionally, considering that a large number of changes of states can also affect the state-of-health of the ESS [28], (15) limits the number of charging/discharging cycles. Finally, constraint (16) defines the value of $SOC_{i,t}$ at the end of the total horizon.

$$P_{i,t}^{BD} = P_{i,t}^{BL} + \sum_{z\in\mathcal{Z}_i}\left(E_{i,z,t}^{T} + E_{i,z,t}^{I}\right)/\Delta t - P_{i,t}^{PV} + \frac{E_{i,t}^{CH}}{\eta_i^{CH}\Delta t} - \frac{\eta_i^{DH}E_{i,t}^{DH}}{\Delta t} \quad \forall i,z,t \ (8)$$

$$Q_{i,t}^{BD} = [P_{i,t}^{BL} + \sum_{z\in\mathcal{Z}_i}\frac{\left(E_{i,z,t}^{T} + E_{i,z,t}^{I}\right)}{\Delta t}]\sqrt{\frac{1}{fp_i^2}-1} \quad \forall i,t \ (9)$$

$$P_{i,t}^{PV} = \eta_i^{PV}A_i^{PV}G_t\left[1-\beta\left(T_t^{Out}-T^{STC}\right)\right] \quad \forall i,t \ (10)$$

$$SOC_{i,t} = SOC_{i,t-1} + \frac{E_{i,t}^{CH} - E_{i,t}^{DH}}{E_i^N} \quad \forall i,t \ (11)$$

$$E_{i,t}^{CH} \le \overline{E}_i^B b_{i,t}^{CH} \quad \forall i,t \ (12)$$

$$E_{i,t}^{DH} \le \overline{E}_i^B b_{i,t}^{DH} \quad \forall i,t \ (13)$$

$$b_{i,t}^{CH} + b_{i,t}^{DH} \le 1 \quad \forall i,t \ (14)$$

$$\sum_{t\in\mathcal{T}}(b_{i,t}^{CH} - (b_{i,t}^{CH} * b_{i,t-1}^{CH})) + (b_{i,t}^{DH} - (b_{i,t}^{DH} * b_{i,t-1}^{DH})) \le \gamma_i \quad \forall i,t \ (15)$$

$$SOC_{i,\mathcal{T}} = SOC^F \quad \forall i \ (16)$$

$$\underline{SOC}_i \le SOC_{i,t} \le \overline{SOC}_i \quad \forall i,t \ (17)$$

$$b_{i,t}^{CH}, b_{i,t}^{DH} \in \{0,1\} \quad \forall i,t \ (18)$$

C. Energy Consumption Model

It is assumed that each zone z is equipped with dimmable lighting appliances controlled simultaneously by the illuminance level set point ($I_{i,z,t}$). Thus, their energy consumption can be expressed as the linear function in (19). In case the zone is unoccupied, then $I_{i,z,t} = 0$ and the lighting energy consumption in the zone is defined as $E_{i,z,t}^{I} = 0$. On the other hand, if the zone is occupied, $I_{i,z,t}$ is subject to operate within the predefined comfortable range $[\underline{\mu o}_{i,z}^{I}, \overline{\mu o}_{i,z}^{I}]$. Recall that the occupancy profile is an input parameter of the model. The term $LP_{i,z}$ represents the lighting power ratio [W/Lx], i.e. the electric power [W] required for reaching the desired illuminance level in [Lx]; which can be obtained through simulations or datasheets.

In addition, each zone is equipped with an HVAC unit comprised by a single speed cooling coil and a constant volume fan. Its consumption is described by (20). Here, the binary variable $u_{i,z,t}$ is used to model the state of the HVAC unit, i. e., $u_{i,z,t} = 1$ if the unit is active, otherwise $u_{i,z,t} = 0$. In (20), $F_{i,z,t}^{RTF}$ represents the fraction of the time step during which the unit works at full capacity, while the second term corresponds to the fan consumption. The total cooling capacity ($q_{i,z,t}^{T}$) and energy input ratio ($F_{i,z,t}^{EIR}$) are adjusted to consider the effect of weather conditions on the nominal cooling capacity ($q_{i,z}^{N}$) and the coefficient of performance ($COP_{i,z}$), using the modifier factors $f_{i,z,t}^{CCT}(q_{i,z,t}^{S})$, $f_{i,z,t}^{EIT}(q_{i,z,t}^{S})$, $f_{i,z,t}^{CCF}$, $f_{i,z,t}^{EIF}$ in (21) and (22). These factors are calculated based on the formulation presented in [29]. Notice that $f_{i,z,t}^{CCT}(q_{i,z,t}^{S})$ and $f_{i,z,t}^{EIRT}(q_{i,z,t}^{S})$ are function of $q_{i,z,t}^{S}$, i. e., the cooling load required by each zone (see Sec.III-D). Constraint (23) establishes the operational limits of each HVAC unit. Finally, the non-manageable demand ($P_{i,t}^{BL}$) of each building is represented by a forecasted power profile.

$$E_{i,z,t}^{I} = LP_{i,z}I_{i,z,t}\Delta t \quad \forall i,z,t \ (19)$$

$$E_{i,z,t}^{T} = q_{i,z,t}^{T}F_{i,z,t}^{EIR}F_{i,z,t}^{RTF}\Delta t + u_{i,z,t}P_{i,z}^{Fan}\Delta t \quad \forall i,z,t \ (20)$$

$$q_{i,z,t}^{T} = f_{i,z,t}^{CCT}(q_{i,z,t}^{S})\cdot f_{i,z,t}^{CCF}\cdot q_{i,z}^{N} \quad \forall i,z,t \ (21)$$

$$F_{i,z,t}^{EIR} = f_{i,z,t}^{EIRT}(q_{i,z,t}^{S})\cdot f_{i,z,t}^{EIRF}/COP_{i,z} \quad \forall i,z,t \ (22)$$

$$u_{i,z,t}\underline{P}_{i,z}^{HVAC}\Delta t \le E_{i,z,t}^{T} \le u_{i,z,t}\overline{P}_{i,z}^{HVAC}\Delta t \quad \forall i,z,t \ (23)$$

$$u_{i,z,t} \in \{0,1\} \quad \forall i,t \ (24)$$

D. Thermal Zone Model

Thermal balance of each zone is defined by (25), based on the model used by EnergyPlus [29]. As presented in Fig.1, the HVAC unit supplies the cooling load $q_{i,z,t}^{S}$ required by the zone, in order to maintain the temperature in the value defined by the set point ($T_{i,z,t}$). Sensible heat gains $q_{i,z,t}^{Oc}$, $q_{i,z,t}^{Ed}$, $q_{i,z,t}^{I}$ take into the account the heat emanated by occupants, electrical devices and lighting appliances, respectively; while $q_{i,z,t}^{Srf}$ represents the heat gain through the zone surfaces. The electrical devices usage ($\kappa_{i,z,t}^{Ed}$) and occupancy ($\kappa_{i,z,t}^{Oc}$) profiles in (26) and (27), can be obtained by forecasting techniques or operational data of the building; while the air volume thermal inertia ($q_{i,z,t}^{Sto}$) and infiltration heat gain ($q_{i,z,t}^{Inf}$) are expressed by (29) and (30), respectively.

$$q_{i,z,t}^{S} = \left(q_{i,z,t}^{Oc} + q_{i,z,t}^{Ed} + q_{i,z,t}^{I}\right) - q_{i,z,t}^{Sto} + q_{i,z,t}^{Inf} + q_{i,z,t}^{Srf} \quad \forall i,z,t \ (25)$$

$$q_{i,z,t}^{Oc} = h^{Oc}\kappa_{i,z,t}^{Oc} \quad \forall i,z,t \ (26)$$

$$q_{i,z,t}^{Ed} = h^{Ed}\kappa_{i,z,t}^{Ed} \quad \forall i,z,t \ (27)$$

$$q_{i,z,t}^{I} = \zeta_{i,z}E_{i,z,t}^{I} \quad \forall i,z,t \ (28)$$

$$q_{i,z,t}^{Sto} = \rho^{Air}c^{Air}\left(T_{i,z,t} - T_{i,z,t-1}\right)v_{i,z} \quad \forall i,z,t \ (29)$$

$$q_{i,z,t}^{Inf} = \rho^{Air}c^{Air}\left(T_t^{out} - T_{i,z,t}\right)\nu_{i,z}^{Inf} \quad \forall i,z,t \ (30)$$

This article has been accepted for publication in a future issue of this journal, but has not been fully edited. Content may change prior to final publication. Citation information: DOI 10.1109/TSG.2018.2822776, IEEE Transactions on Smart Grid

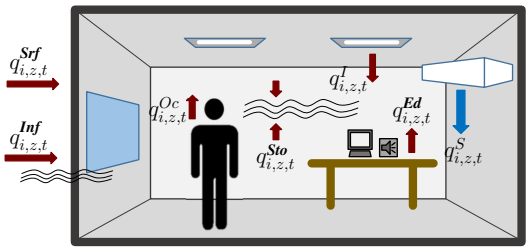

Figure 1. Heat gains considered in the thermal balance of each zone.

E. Comfort Model

Lighting appliances and HVAC units are managed by the BEMS to achieve energy saving. However, this management must consider the indoor conditions to guarantee the occupants' comfort. To do this, the global comfort index ($C_{i,z}$) in (31) can be used, which is based on the model proposed in [26], [30]. This index calculates the average of the thermal ($C^T_{i,z,t}$) and visual factor ($C^I_{i,z,t}$) during the total occupied period of each zone $\tau\kappa^{Oc}_{i,z}$. Based on this definition, $C_{i,z}$ equal 1 means that comfortable set points are strictly accomplished. Factors $C^T_{i,z,t}$ and $C^I_{i,z,t}$ quantify the deviation from the comfortable predefined values, as modeled in (32) and (33). These deviations are based on the difference between the current set points and the comfortable predefined conditions, as defined in (34) and (35), and are considered only when the zone is occupied. Finally, (36) establishes the minimum permissible comfort $\underline{C}_i$, meanwhile constraints (37) and (38) keep $T_{i,z,t}$ and $I_{i,z,t}$ within comfortable ranges.

$$C_{i,z} = \frac{1}{\tau\kappa^{Oc}_{i,z}} \sum_{t\in\mathcal{T}^{\kappa}_{i,z}} \left(\omega^T C^T_{i,z,t}\right) + \left(\omega^I C^I_{i,z,t}\right) \qquad \forall i,z,t \quad (31)$$

$$C^T_{i,z,t} = 1 - \left(\Delta^T_{i,z,t}/\mu o^T_{i,z}\right)^2 \qquad \forall i,z,t \quad (32)$$

$$C^I_{i,z,t} = 1 - \left(\Delta^I_{i,z,t}/\mu o^I_{i,z}\right)^2 \qquad \forall i,z,t \quad (33)$$

$$\Delta^T_{i,z,t} = T_{i,z,t} - \mu o^T_{i,z} \qquad \forall i,z,t \quad (34)$$

$$\Delta^I_{i,z,t} = I_{i,z,t} - \mu o^I_{i,z} \qquad \forall i,z,t \quad (35)$$

$$C_{i,z} \geq \underline{C}_i \qquad \forall i,z \quad (36)$$

$$\underline{\mu o}^T_{i,z} \leq T_{i,z,t} \leq \overline{\mu o}^T_{i,z} \qquad \forall i,z,t \quad (37)$$

$$\underline{\mu o}^I_{i,z} \leq I_{i,z,t} \leq \overline{\mu o}^I_{i,z} \qquad \forall i,z,t \quad (38)$$

Notice that the effect of the global irradiance over the indoor illuminance level has not been considered in (38). However, this can be easily included if (38) is re-written as,

$$\underline{\mu o}^I_{i,z} \leq I_{i,z,t} + I^N_{i,z,t} \leq \overline{\mu o}^I_{i,z}, \quad \forall i,z,t, \qquad (39)$$

where $I^N_{i,z,t}$ represents the external/natural component of the illuminance level of each zone, which can be handled as an input parameter.

IV. Proposed MILP Model and Solution Strategy

Finding an optimal solution to the MINLP model (1)–(38) is not easy due to the nature of the decision variables and complex methods used to estimate $f^{CCT}_{i,z,t}(q^S_{i,z,t})$, $f^{EIT}_{i,z,t}(q^S_{i,z,t})$ in (21) and (22), and $q^{Srf}_{i,z,t}$ in (25). Additionally, the use of non-linear optimization techniques do not guarantee optimality. Due to this, a strategy to simplify the original MINLP model is proposed. This strategy is composed by two stages: a pre-processing and an optimization stage, as explained next.

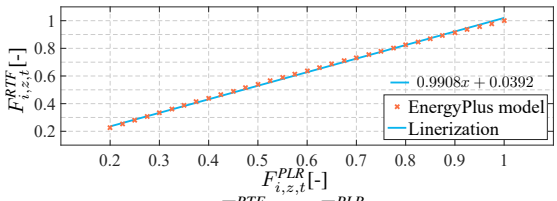

Figure 2. Relation between $F^{RTF}_{i,z,t}$ and $F^{PLR}_{i,z,t}$.

A. Pre-processing Stage

This stage is used to approximate $f^{CCT}_{i,z,t}(q^S_{i,z,t})$, $f^{EIT}_{i,z,t}(q^S_{i,z,t})$, and $q^{Srf}_{i,z,t}$, using a set of equivalent representations obtained through simulations executed in EnergyPlus. At the beginning of the total horizon, each building is simulated using fixed set points $I^o_{i,z,t}$, $T^o_{i,z,t}$, and weather forecasting information. The results obtained are used to approximate $f^{CCT}_{i,z,t}(q^S_{i,z,t})$ and $f^{EIT}_{i,z,t}(q^S_{i,z,t})$ in (21) and (22). This approximation is suitable since constraints (37) and (38) keep the indoor conditions within predefined thresholds during the optimization process.

In (20), $F^{RTF}_{i,z,t}$ can be approximated by the expression in (40), obtained through a linear regression, based on the model used by EnergyPlus in [29]. This approximation introduces a low error since the relation between $F^{RTF}_{i,z,t}$ and the part load ratio ($F^{PLR}_{i,z,t}$) is almost linear in the operational range of the HVAC unit, as shown in Fig.2. Following the model used by EnergyPlus, in (41), $F^{PLR}_{i,z,t}$ is defined as a function of the sensible cooling load required by the zone ($q^S_{i,z,t}$), the ventilation heat gain ($q^{Ven}_{i,z,t}$) and thermal losses ($q^{Loss}_{i,z,t}$). The sensible heat ratio modifier factor ($f^{SHR}_{i,z,t}$) is estimated using the formulation in [31] and the results of the simulation. Finally, the ventilation heat gain is defined as in (42), while thermal losses are presented in (43).

$$F^{RTF}_{i,z,t} = \psi' F^{PLR}_{i,z,t} + \psi'' \qquad \forall i,z,t \quad (40)$$

$$F^{PLR}_{i,z,t} = \frac{q^S_{i,z,t} + q^{Ven}_{i,z,t} + q^{Loss}_{i,z,t}}{f^{SHR}_{i,z,t} F^{SHR}_{i,z} q^T_{i,z,t}} \qquad \forall i,z,t \quad (41)$$

$$q^{Ven}_{i,z,t} = \rho^{Air} c^{Air} \left(T^{Out}_t - T_{i,z,t}\right) \nu^{Fan}_{i,z} u_{i,z,t} \qquad \forall i,z,t \quad (42)$$

$$q^{Loss}_{i,z} = \left(1 - \eta^{Fan}\right) P^{Fan}_{i,z} u_{i,z,t} + \rho^{Air} c^{Air} \delta^{T_{Fan}} \nu^{Fan}_{i,z} \qquad \forall i,z,t \quad (43)$$

The heat through the surfaces ($q^{Srf}_{i,z,t}$) in (25) is approximated by the linear function defined in (44). This expression is based on the heat through the surfaces obtained in the simulation ($q^{Srfo}_{i,z,t}$), which is adjusted according to the difference between the temperature set point used in the simulation ($T^o_{i,z,t}$) and the temperature set point ($T_{i,z,t}$), defined during the optimization process. $\delta^{Srf}_{i,z,t}$ represents the surfaces heat gain variation when $T_{i,z,t}$ changes 1^oC with respect to $T^o_{i,z,t}$. In order to obtain this parameter, two additional simulations using the temperature set points ($T^o_{i,z,t} - 1^oC$) and ($T^o_{i,z,t} + 1^oC$) are required.

$$q^{Srf}_{i,z,t} = q^{Srfo}_{i,z,t} + \left(T^o_{i,z,t} - T_{i,z,t}\right) \delta^{Srf}_{i,z,t} \qquad \forall i,z,t \quad (44)$$

B. Optimization Stage

Before stating the final optimization model, linear representations are presented to approximate the non-linear terms of the original MINLP model.

This article has been accepted for publication in a future issue of this journal, but has not been fully edited. Content may change prior to final publication. Citation information: DOI 10.1109/TSG.2018.2822776, IEEE Transactions on Smart Grid

1) Electrical Grid Linear Formulation: Equations (2)–(5) can be linearized by introducing the variables $V_{i,t}^{sqr}$, $I_{ij,t}^{sqr}$ to represent $V_{i,t}^2$ and $I_{ij,t}^2$; meanwhile, quadratic terms $P_{ij,t}^2$ and $Q_{ij,t}^2$, can be approximate by the piecewise linear formulation described in (45)–(53), which is based on the discretization for quadratic expressions presented in [32]. Here, $\delta_{ij}^P = \overline{P}_{ij}/\overline{\lambda}$ and $\delta_{ij}^Q = \overline{Q}_{ij}/\overline{\lambda}$. Other linear formulations for the power flow modeling can be used as well, such as the ones presented in [33], [34].

$$P_{ij,t} = P_{ij,t}^+ - P_{ij,t}^- \qquad \forall ij,t \quad (45)$$

$$Q_{ij,t} = Q_{ij,t}^+ - Q_{ij,t}^- \qquad \forall ij,t \quad (46)$$

$$P_{ij,t}^+ + P_{ij,t}^- = \sum\nolimits_{\lambda=1}^{\overline{\lambda}} \delta_{ij,t,\lambda}^P \qquad \forall ij,t \quad (47)$$

$$Q_{ij,t}^+ + Q_{ij,t}^- = \sum\nolimits_{\lambda=1}^{\overline{\lambda}} \delta_{ij,t,\lambda}^Q \qquad \forall ij,t \quad (48)$$

$$0 \leq \delta_{ij,t,\lambda}^P \leq \overline{\delta}_{ij}^P \qquad \forall ij,t,\lambda = 1...\overline{\lambda} \quad (49)$$

$$0 \leq \delta_{ij,t,\lambda}^Q \leq \overline{\delta}_{ij}^Q \qquad \forall ij,t,\lambda = 1...\overline{\lambda} \quad (50)$$

$$P_{ij,t}^+, P_{ij,t}^-, Q_{ij,t}^+, Q_{ij,t}^- \geq 0 \qquad \forall ij,t \quad (51)$$

$$\sigma_{ij,\lambda}^P = (2\lambda - 1)\overline{\delta}_{ij}^P \qquad \forall ij,\lambda = 1...\overline{\lambda} \quad (52)$$

$$\sigma_{ij,\lambda}^Q = (2\lambda - 1)\overline{\delta}_{ij}^Q \qquad \forall ij,\lambda = 1...\overline{\lambda} \quad (53)$$

Additionally, $V_{i,t}^{sqr}$ can be replaced by its estimation $(V'_{i,t})^2$, in order to approximate the product of variables $V_{i,t}^{sqr}$ and $I_{ij,t}^{sqr}$ on the left-hand side of (5). This simplification introduces a relatively low error since the operational range for the voltage magnitude $[\underline{V}, \overline{V}]$ is small [35]. Then, (5) can be rewritten as the linear expression,

$$(V'_{i,t})^2 I_{ij,t}^{sqr} = (\sum_{\lambda=1}^{\overline{\lambda}} \sigma_{ij,\lambda}^P \delta_{ij,t,\lambda}^P) + (\sum_{\lambda=1}^{\overline{\lambda}} \sigma_{ij,\lambda}^Q \delta_{ij,t,\lambda}^Q) \quad \forall ij,t \quad (54)$$

2) ESS Linear Formulation: The product $b_{i,t}^{CH} \cdot b_{i,t-1}^{CH}$ in (15) can be replaced by the auxiliary variable $\Gamma_{i,t}^{CH}$, which is subject to (55)–(57). A similar approach can be carried out to linearize the product $b_{i,t}^{DH} \cdot b_{i,t-1}^{DH}$.

$$\Gamma_{i,t}^{CH} \leq b_{i,t}^{CH} \qquad \forall i,t \quad (55)$$

$$\Gamma_{i,t}^{CH} \leq b_{i,t-1}^{CH} \qquad \forall i,t \quad (56)$$

$$b_{i,t-1}^{CH} + b_{i,t-1}^{CH} - 1 \leq \Gamma_{i,t}^{CH} \qquad \forall i,t \quad (57)$$

3) Comfort Linear Formulation: The quadratic term $(\Delta_{i,z,t}^T)^2$ in (32), can be linearized using the piecewise linear representation described in (58)–(63), where $\delta_{i,z}^T = (\overline{\mu o}_{i,z}^T - \underline{\mu o}_{i,z}^T)/\overline{\lambda}$ and $\delta_{i,z}^I = (\overline{\mu o}_{i,z}^I - \underline{\mu o}_{i,z}^I)/\overline{\lambda}$. A similar approach can be used to linearize $(\Delta_{i,z,t}^I)^2$ in (33).

$$C_{i,z,t}^T = 1 - (\sum\nolimits_{\lambda=1}^{\overline{\lambda}} \sigma_{i,z,\lambda}^T \delta_{i,z,t,\lambda}^T)/(\mu o_{i,z}^T)^2 \qquad \forall i,z,t \quad (58)$$

$$\Delta_{i,z,t}^T = \Delta_{i,z,t}^{T+} - \Delta_{i,z,t}^{T-} \qquad \forall i,z,t \quad (59)$$

$$\Delta_{i,z,t}^{T+} + \Delta_{i,z,t}^{T-} = \sum\nolimits_{\lambda=1}^{\overline{\lambda}} \delta_{i,z,t,\lambda}^T \qquad \forall i,z,t \quad (60)$$

$$0 \leq \delta_{i,z,t,\lambda}^T \leq \overline{\delta}_{i,z}^T \qquad \forall i,z,t,\lambda = 1...\overline{\lambda} \quad (61)$$

$$\Delta_{i,z,t}^{T+}, \Delta_{i,z,t}^{T-} \geq 0 \qquad \forall i,z,t \quad (62)$$

$$\sigma_{i,z,\lambda}^T = (2\lambda - 1)\overline{\delta}_{i,z}^T \qquad \forall z,\lambda = 1...\overline{\lambda} \quad (63)$$

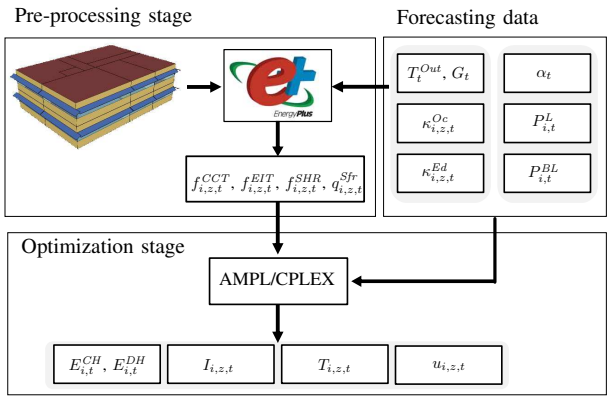

Figure 3. Solution strategy comprising a pre-processing and an optimization stage.

4) Ventilation Heat Gain Linear Formulation: The product $T_{i,z,t} \cdot u_{i,z,t}$ in (42), can be replaced by the variable $\Phi_{i,z,t}^T$ as in (64). Then, $\Phi_{i,z,t}^T$ can be represented by the disjunctive formulation defined in (65) and (66).

$$q_{i,z,t}^{Ven} = \rho^{Air} c^{Air} \nu_{i,z}^{Fan} (T_t^{Out} u_{i,z,t} - \Phi_{i,z,t}^T) \qquad \forall i,z,t \quad (64)$$

$$-\overline{\mu o}_{i,z}^T u_{i,z,t} \leq \Phi_{i,z,t}^T \leq \overline{\mu o}_{i,z}^T u_{i,z,t} \qquad \forall i,z,t \quad (65)$$

$$-\overline{\mu o}_{i,z}^T (1 - u_{i,z,t}) \leq \Phi_{i,z,t}^T - T_{i,z,t} \leq \overline{\mu o}_{i,z}^T (1 - u_{i,z,t}) \qquad \forall i,z,t \quad (66)$$

C. Overview of the Solution Strategy and Proposed MILP model

The proposed strategy is presented in Fig. 3. First, forecasting information about energy price, non-manageable loads of the microgrid, weather conditions, electrical devices usage and occupancy profiles, and non-manageable loads of buildings is gathered. Then, the pre-processing stage is executed for each building as explained in Sec.IV-A. Finally, the microgrid's operator executes the optimization stage using the models presented in Sec.IV-B. The resulting MILP model solved in this stage can be described as:

$$\min \quad (1),$$

where $I_{ij,t}^{sqr} \simeq I_{ij,t}^2$ subject to: (2)–(4), (6)–(11), (14)–(22), (25)–(31), (34)–(38), (40)–(66).

D. Communication Requirements

In order to implement the proposed strategy, two-way communication channels are required between the BEMS of the buildings and the microgrid's operator. These communication requirements can be addressed by using a multi-agents architecture, supported by a cloud-based infrastructure such as the one proposed in [36]. Moreover, a data workflow management, similar to the one described in [37], can be also developed in order to reduce the complexity in the collecting and sending process of all the data exchanged between the microgrid's operator and the buildings.

This article has been accepted for publication in a future issue of this journal, but has not been fully edited. Content may change prior to final publication. Citation information: DOI 10.1109/TSG.2018.2822276, IEEE Transactions on Smart Grid

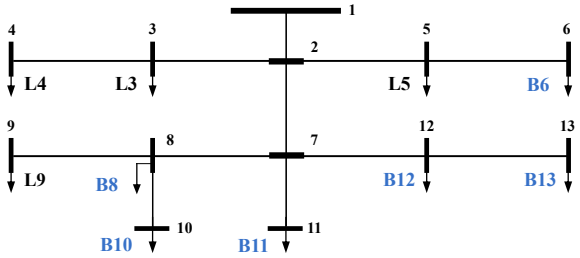

Figure 4. Microgrid test case, L represents non-manageable loads and B represents the buildings.

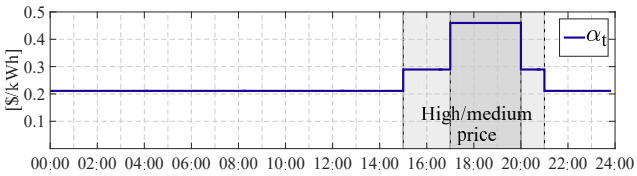

Figure 5. Energy price signal.

V. Test Case and Discussion

The proposed model was tested in the 13-bus synthetic microgrid shown in Fig. 4, information related to microgrid can be found in [38]. Fig. 5 shows the energy price scheme, which corresponds to the energy tariff of the southeast region of Brazil [39]. Table I summarizes buildings general information. For all buildings, predefined comfortable set points were defined as $\mu o^T_{i,z} = 22.5^o$C and $\mu o^I_{i,z} = 500$Lx, as presented in Table II. Temperature and illuminance were subject to operate within $[20-25]^o$C and $[400-600]$Lx, respectively. The voltage thresholds $\underline{V}$ and $\overline{V}$ were defined as 0.93 and 1.05, respectively. The total horizon (24h) is analyzed using 10 min time steps. A database containing real weather information provided in [40] was used. The MILP model was implemented in AMPL [41], and solved with CPLEX [42], using a workstation with an Intel i7-4790 processor and 16 GB RAM.

Five cases were implemented, described as,

Case I:	Only consumption management, individualist scheme,
Case II:	Only consumption management, centralized scheme,
Case III:	Consumption management, PV, ESS, individualist scheme,
Case IV:	Consumption management, PV, ESS, centralized scheme,
Case IV-RH:	Same as Case IV with the proposed RH scheme.

Cases I to IV were solved with a deterministic approach, assuming that forecasting information describes a perfect knowledge of real conditions. Case IV-RH is solved with the RH scheme presented in the Appendix. In Cases I and III each building optimizes its own operation in an individualist strategy, i. e., without considering the grid or other buildings. In Cases II and IV the microgrid's operator optimizes, in a centralized fashion, the buildings energy consumption and the microgrid. In all cases, the minimum permissible comfort index $\underline{C}_i$ was defined as 0.995.

Table I
Buildings General Information

	B6 / B11	B8 / B12	B10 / B13	Units
Usage	Classrooms	Technology	Offices	—
Operating time	[7:00-21:00]	[8:00-18:00]	[8:00-18:00]	—
A_{PV}	210	260	200	$[m^2]$
E^B	70	88	68	[kWh]
Zones	10	10	10	—

Table II
Comfortable Indoor Conditions.

	Typical set point	Comfortable range
Temperature* [^{o}C]	$\mu o^T_{i,z} = 22.5$	$[\underline{\mu o}^T_{i,z}, \overline{\mu o}^T_{i,z}] = [20, 25]$
Illuminance** [Lx]	$\mu o^I_{i,z} = 500$	$[\underline{\mu o}^I_{i,z}, \overline{\mu o}^I_{i,z}] = [400, 600]$

* Conditions for a summer day according to [43].
** Conditions for desk tasks according to [44].

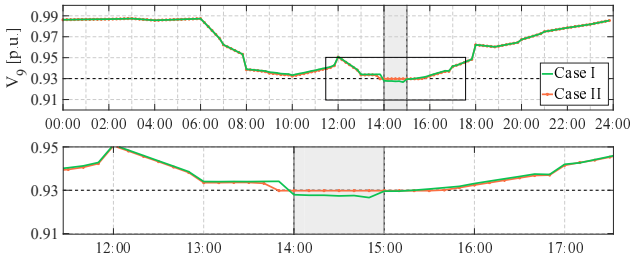

Figure 6. Voltage at bus 9 for the total horizon. Case I and II.

A. Buildings Consumption Management Capacity

Cases I and II do not include PV and ESS into the analysis in order to assess the buildings consumption management capacity. In Case I, where each building optimizes its operation individually, the voltage at bus 9 drops below the minimum limit at 14:00h, as shown in Fig. 6. In contrast, in Case II, the voltage profile is improved due the coordinated action of the BEMSs of all buildings, executed by the microgrid's operator.

The coordinated action of BEMSs is based on the management of HVAC units and lighting appliances. To show this, Fig. 7 presents the temperature and illuminance level set points of building B10. For Case II, the HVAC unit is activated at 13:50h with the minimum temperature (20^oC) to pre-cool the zone before it becomes occupied at 14:00h. Additionally, between 14:00-15:00h, temperature is defined to the maximum value (25^oC), while the illuminance level is reduced. Most of the zones in all buildings operate in a similar fashion during the same time period, as a consequence, power demand of buildings B6, B8, B10 decrease (in average) 6%, 10.3% and 11.1%, respectively, when comparing with Case I. Buildings B11, B12 and B13 described similar results. In total, the power consumption of buildings and power losses is reduced by 8.5%, allowing the microgrid's operator to meet the microgrid voltage constraint.

Notice in Fig. 7 for Case II, that during the time periods before 14:00h and after 15:00h, HVAC units operate with lower temperature values and lighting appliances with higher illuminance level, when compared with Case I. As a consequence, the power consumption of buildings is increased, as can be seen in Fig. 8. The rationale behind these management decisions is to meet the comfort constraint at the end of the

This article has been accepted for publication in a future issue of this journal, but has not been fully edited. Content may change prior to final publication. Citation information: DOI 10.1109/TSG.2018.2822276, IEEE Transactions on Smart Grid

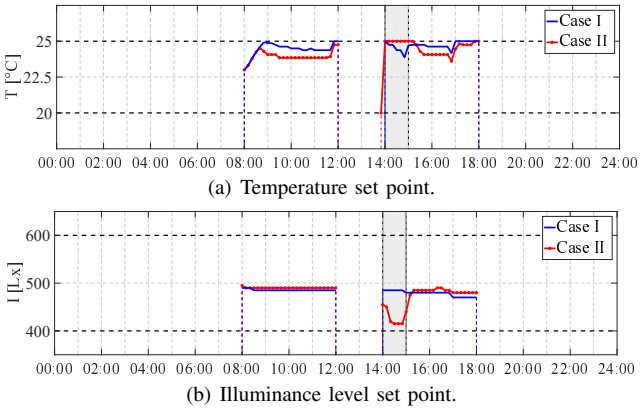

(a) Temperature set point.

(b) Illuminance level set point.

Figure 7. Temperature and illuminance set points of zone 10, in building B10 during the occupied periods.

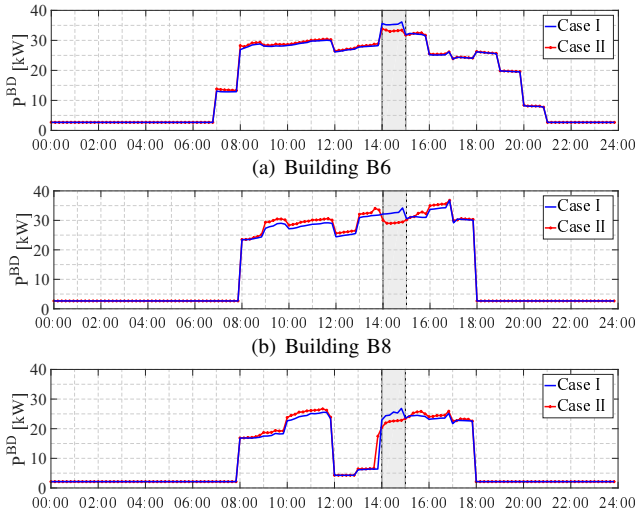

(a) Building B6

(b) Building B8

(c) Building B10

Figure 8. Buildings power consumption for the total horizon. Case I and II.

total horizon. In total, the energy consumption in Case II is 1.3% higher than in Case I, the cost of the buildings operation increased 1.4% and power losses cost 0.5%. Nevertheless, this operation guarantees the voltage constraint of the grid. A general comparison of both cases is presented in Table III.

The comfort constraint in (36) plays an important role in the management decisions, as it can be seen in Table IV. In fact, if the constraint is relaxed to $\underline{C}_i = 0.90$, a solution with a total cost 7.8% lower than the base case ($\underline{C}_i = 0.995$), can be obtained. On the other hand, and depending on the conditions, if the management capabilities are limited ($\underline{C}_i = 1$), a high cost and technically unfeasible solution, can be obtained.

B. Buildings Operation with PV and ESS

Fig. 9 depicts the voltage magnitude profile at bus 9 for Cases III and IV. In both cases, the microgrid operates within the voltage magnitude limits, since PV generation supplies locally a portion of the buildings consumption. As presented in Table III, the energy consumption, the buildings operation cost and the power losses cost are equivalent in both cases. However, as shown in Fig. 10, in Case IV the power demand of buildings and the power losses are reduced in the morning, between 8:00h and 12:00h, shifting the demand to earlier hours. Particularly, the power peak is reduced by 15.3% in Case IV, when compared with Case III. In this case, this

Table III
COMPARISON RESULTS FOR CASES I, II, III AND IV ($\underline{C}_i = 0.995$)

	Case I	Case II	Case III	Case IV
Consumption [kWh]	2217.7	2246.7	1368.4	1362.7
Total Cost [$]	579.5	586.8	321.1	319.8
Peak power [kW]	230.1	215.6	202.7	171.8
Buildings operation cost [$]	487.0	493.8	244.1	244.2
Power losses cost [$]	92.5	93.0	77.0	75.6
Power losses [%]	2.89	2.91	2.64	2.59
V [p.u]	0.926	0.930	0.933	0.936

Table IV
CASE II WITH DIFFERENT VALUES OF $\underline{C}_i$

$\underline{C}_i$	0.900	0.995	1
Consumption [kWh]	2060.3	2246.7	2466.8
Total Cost [$]	540.6	586.8	645.8
Peak power [kW]	201.72	215.6	247.6
V [p.u]	0.930	0.930	0.926

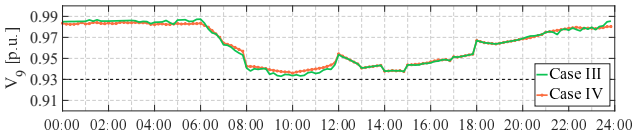

Figure 9. Voltage at bus 9 for the total horizon. Case III and IV.

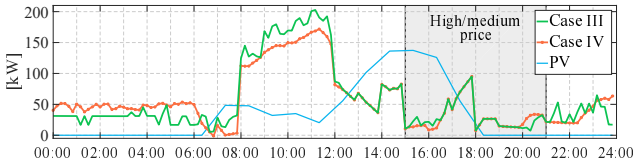

Figure 10. Buildings demand and power losses. Case III and IV.

result is not related to the management of HVAC and lighting appliances but instead to the ESS operation. To see this, observe in Fig. 11, that in Case IV the charging operation of the ESS in buildings B6, B8 and B10 is completely shifted to early in the morning. Buildings B11, B12, B13 described similar results. Finally, as was expected, during the medium/high price period from 15:00h to 21:00h, the power demand of buildings and losses decreased due that the ESS operates in discharging mode.

In general, the pre-processing stage of a single building was executed in 24s, approximately. It is important to remind this stage is executed in advance, i.e., at the beginning of the time horizon. In Case IV, considering that the microgrid's operator solves the entire problem in a centralized fashion, the pre-processing stage of all buildings (6 in total) was executed in 144s, while the processing time of the optimization stage was about 270s.

To assess the error of the proposed strategy, the operation of each building was simulated in EnergyPlus using the values of $T_{i,z,t}$, $I_{i,z,t}$ and $u_{i,z,t}$ obtained solving the MILP model. This procedure allows obtaining the consumption profiles of the buildings. Using these results, the microgrid operation was estimated solving the non-linear power flow formulation in Sec.III-A. According to this, the maximum error for all buildings was near to 4.5% when comparing the consumption obtained with the MILP model and EnergyPlus. Additionally, an error of 1.5% was observed for the total cost.

This article has been accepted for publication in a future issue of this journal, but has not been fully edited. Content may change prior to final publication. Citation information: DOI 10.1109/TSG.2018.2822276, IEEE Transactions on Smart Grid

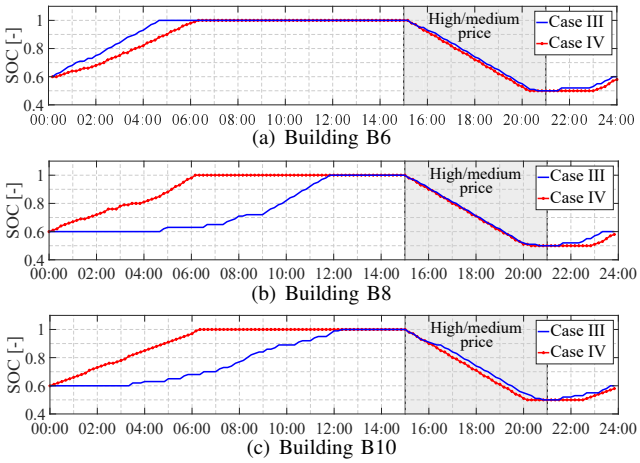

Figure 11. SOC of the ESS for buildings B6, B8 and B10. Case III and IV.

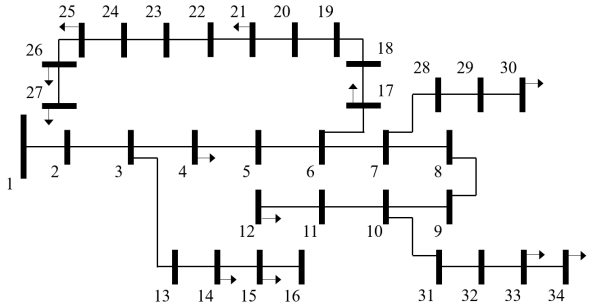

Figure 12. 34-bus microgrid test case, arrows represent buildings; non-manageable loads are not showed.

C. Large-size Case of Study

In order to test the scalability of the proposed strategy, a larger-size case of study is analyzed in this section. For this, the 34-bus microgrid shown in Fig. 12 is considered, including 17 non-manageable loads, and 12 buildings equipped with PV and ESS. Detailed information regarding the microgrid can be found in [45]. In this case, the centralized scheme is applied, using a minimum permissible comfort index of $\underline{C}_i = 0.995$.

Fig. 13 shows all buildings power consumption, including also the power losses. In general, all buildings describe equivalent results to the ones found for the 13-bus microgrid in Case IV, managing HVAC and lighting appliances to reduce the energy consumption. As expected, during the medium/high price period from 15:00h to 21:00h, the power demand of buildings and losses are reduced due to the discharging operation of ESS.

In this large-size case, the pre-processing stage required about 288s, in contrast with the 144s required for the 13-bus microgrid in Case IV. This increase is due to the higher number of buildings considered in the large-size case. On the other hand, the processing time of the optimization stage for the large-size case was near to 290s, which is close to the processing time (270s) of the 13-bus microgrid in Case IV, showing the effectiveness of the proposed strategy to handle larger-size cases without a significant increase in the processing time of the optimization stage. Finally, relative errors in the same order of magnitude (4.4% for all buildings, when comparing the consumption obtained with the MILP model and EnergyPlus) were also obtained in this case.

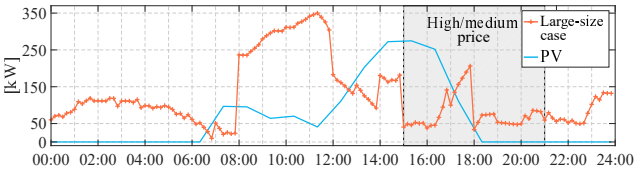

Figure 13. Buildings demand and power losses for the large-size case.

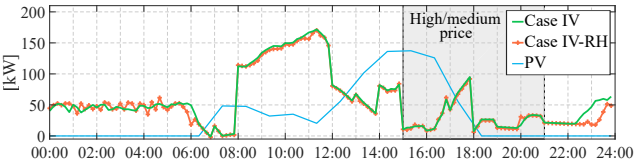

Figure 14. Buildings demand and power losses. Comparison Case IV (deterministic) and Case IV-RH (considering uncertainty).

Table V
COMPARISON RESULTS FOR CASES IV AND IV-RH ($\underline{C}_i = 0.995$).

	Case IV	Case IV-RH	Traditional RH
Consumption [kWh]	1362.7	1311.0	1305.1
Total Cost [$]	319.8	307.7	306.1
Peak power [kW]	171.8	170.2	170.9
Mean processing time [s]	270	7	580
Forecasts (for each variable) [-]	144	28	144

D. Uncertainty Consideration

In order to consider uncertainty in G_t, T_t^{Out}, and $\kappa_{i,z,t}^{Oc}$, Case IV-RH uses the RH scheme presented in the Appendix. Fig. 14 shows the comparison between the solution found in Case IV, applying the deterministic approach, and the solution found by the RH strategy in Case IV-RH. Notice that, the power consumption of buildings and power losses is similar in both cases. In Case IV-RH, the total cost at the end of the day differs by 3.8% from the solution found through the deterministic approach assuming perfect knowledge of the conditions (see Table V). This difference is due that in the proposed RH scheme the constraint (16) is not considered, since the end of the total horizon is rolled at each time step. The mean processing time of the optimization stage to solve the problem for the total horizon in Case IV-RH is approximately 7s.

In order to show the effectiveness of the proposed RH scheme, a comparison with a traditional RH scheme[3] is carried out. Table V summarizes the main results. Notice that the total cost for the traditional RH scheme differs by 0.5% from the solution found using the proposed RH scheme; which suggests that both solutions are similar in terms of the management decisions. However, notice that the mean processing time of the optimization stage required by the proposed RH scheme is significantly lower (near to 7s) in contrast to the 580s required by the traditional RH scheme. Finally, it is important to highlight that the proposed RH scheme requires less forecast information. In fact, the traditional RH strategy uses 144 forecasts for each variable at each time step, in contrast to the 28 values (for each variable) required by the proposed RH scheme.

[3]The traditional RH scheme uses uniform time steps in a rolling horizon window that stays constant throughout the procedure, see [25] for further details.

This article has been accepted for publication in a future issue of this journal, but has not been fully edited. Content may change prior to final publication. Citation information: DOI 10.1109/TSG.2018.2822276, IEEE Transactions on Smart Grid

VI. Conclusion

A detailed MINLP model to describe the operation of multiple buildings in a microgrid, was presented. Additionally, a strategy that simplifies the original model was proposed, based on a set of linearization techniques and equivalent representations, obtained through a pre-processing stage executed in EnergyPlus. The proposed approach allows optimizing, in a centralized fashion, the buildings and microgrid operation. According to the results, including the electrical grid operation in the management problem allows the microgrid's operator to take advantage of the buildings management capacity to guarantee the technical constraints of the microgrid, while the BEMS of each building ensures the comfortable conditions for the occupants. Acceptable errors were obtained when compared the proposed strategy with the original formulation.

Appendix
Rolling Horizon Scheme

The proposed RH strategy is presented in Fig. 15. The total horizon is divided into two periods: a short horizon, with length T^S and discretized time steps of length Δt^S; and a long horizon, with length T^L and time steps of length Δt^L. Notice that, the first time step of the short horizon corresponds to the control stage (t^C). The pre-procesing stage is executed in advance at the beginning of the total horizon. At instant t the measures and forecasts of variables G_t, T_t^{Out}, and $\kappa_{i,z,t}^{Oc}$ are updated; uncertainty in other variables such as the energy price, non-manageable building loads demand, among others, can be also considered, including their forecasts and measures at each time step. Then, the optimization stage is executed and the solution is implemented. At instant $t+\Delta t^S$, t^C and T^S are redefined and the problem is solved again. At instant T^S, the total window horizon is rolled Δt^L ahead, and t^C, T^S, T^L are redefined. It is important to highlight that the pre-processing stage is executed again when the total horizon (24h) has been analyzed, in order to update the approximation of $f_{i,z,t}^{CCT}$, $f_{i,z,t}^{EIT}$, $f_{i,z,t}^{SHR}$, and $q_{i,z,t}^{Srf}$.

The short length of Δt^S allows capturing significant variations related to weather conditions, zone thermal inertia and other variables such as occupancy, in the time steps near to t^C. Particularly, for the buildings analyzed in the test cases, the zones take between 10 and 20min to reach the temperature set point defined by the HVAC units, thus, Δt^S can be defined as 10min to capture these thermal dynamics. This time step length is in agreement with the one defined in related works such as [24], [46]. On the other hand, considerable changes in building operation occur at the beginning of the hours. For instance, offices buildings open at 08:00, lunchtime starts 12:00 and so forth. Thus, defining $\Delta t^L = 1$h makes the time steps of the long horizon to coincide with the beginning of the following hours, capturing the significant changes of buildings operation.

The main advantage of the proposed RH scheme is that it reduces the computation cost and the amount of forecasting information. Analyzing only the short horizon with discretized intervals allows the microgrid's operator to reduce the processing time of the optimization problem stage. Besides, when $\Delta t^S = 10$min and $\Delta t^L = 1$h, the microgrid's operator requires only 28 forecasts for each variable, instead of the 144 values which would be used by a traditional RH technique.

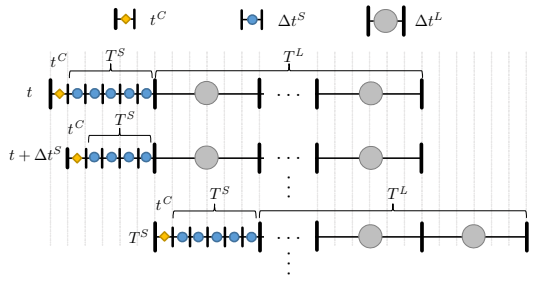

Figure 15. Rolling horizon (RH) scheme. In Case IV-RH, total horizon is 24h, $\Delta t^S = 10$min and $\Delta t^L = 1$h.

References

[1] N. Liu, Q. Chen, J. Liu, X. Lu, P. Li, J. Lei, and J. Zhang, "A heuristic operation strategy for commercial building microgrids containing evs and pv system," *IEEE Trans. Ind. Electron.*, vol. 62, no. 4, pp. 2560–2570, Apr. 2015.

[2] S. Deng, R. Wang, and Y. Dai, "How to evaluate performance of net zero energy building – a literature research," *Energy*, vol. 71, pp. 1 – 16, Jul. 2014.

[3] H. Hao, C. D. Corbin, K. Kalsi, and R. G. Pratt, "Transactive control of commercial buildings for demand response," *IEEE Trans. Power Syst.*, vol. 32, no. 1, pp. 774–783, Jan. 2017.

[4] T. Samad, E. Koch, and P. Stluka, "Automated demand response for smart buildings and microgrids: The state of the practice and research challenges," *Proc. IEEE*, vol. 104, no. 4, pp. 726–744, Apr. 2016.

[5] F. Rahimi and A. Ipakchi, "Using a transactive energy framework: Providing grid services from smart buildings," *IEEE Electrific. Mag.*, vol. 4, no. 4, pp. 23–29, Dec. 2016.

[6] M. K. Muthalib and C. O. Nwankpa, "Physically based building load model for electric grid operation and planning," *IEEE Trans. Smart Grid*, vol. 8, no. 1, pp. 169–177, Jan. 2017.

[7] S. Hanif, T. Massier, H. B. Gooi, T. Hamacher, and T. Reindl, "Cost optimal integration of flexible buildings in congested distribution grids," *IEEE Trans. Power Syst.*, vol. 32, no. 3, pp. 2254–2266, May 2017.

[8] D. Sturzenegger, D. Gyalistras, M. Morari, and R. S. Smith, "Model predictive climate control of a Swiss office building: Implementation, results, and cost-benefit analysis," *IEEE Trans. Control Syst. Technol.*, vol. 24, no. 1, pp. 1–12, Jan. 2016.

[9] Z. Xu, X. Guan, Q. S. Jia, J. Wu, D. Wang, and S. Chen, "Performance analysis and comparison on energy storage devices for smart building energy management," *IEEE Trans. Smart Grid*, vol. 3, no. 4, pp. 2136–2147, Dec. 2012.

[10] A. A. Aizpuru, "Energy production and consumption scheduling in smart buildings," Master's thesis, School of Energy, Environment and Agryfood, Cranfield Univ., Cranfield, UK, 2016.

[11] C. D. Korkas, S. Baldi, I. Michailidis, and E. B. Kosmatopoulos, "Occupancy-based demand response and thermal comfort optimization in microgrids with renewable energy sources and energy storage," *Applied Energy*, vol. 163, no. 1, pp. 93 – 104, Feb. 2016.

[12] S. Baldi, A. Karagevrekis, I. T. Michailidis, and E. B. Kosmatopoulos, "Joint energy demand and thermal comfort optimization in photovoltaic-equipped interconnected microgrids," *Energy Convers. Manage.*, vol. 101, no. 1, pp. 352 – 363, Sep. 2015.

[13] R. Bălan, J. Cooper, K.-M. Chao, S. Stan, and R. Donca, "Parameter identification and model based predictive control of temperature inside a house," *Energy and Buildings*, vol. 43, no. 2-3, pp. 748 – 758, Feb. 2011.

[14] J. Y. Joo and M. D. Ilić, "An information exchange framework utilizing smart buildings for efficient microgrid operation," *Proc. IEEE*, vol. 104, no. 4, pp. 858–864, Apr. 2016.

[15] B. Verbruggen and J. Driesen, "Grid impact indicators for active building simulations," *IEEE Trans. Sustain. Energy*, vol. 6, no. 1, pp. 43–50, Jan. 2015.

[16] G. R. Bharati, M. Razmara, S. Paudyal, M. Shahbakhti, and R. D. Robinett, "Hierarchical optimization framework for demand dispatch in building-grid systems," in *2016 IEEE Power and Energy Society General Meeting (PESGM)*, July 2016, pp. 1–5.

[17] B.-L. Ahn, S. Yoo, J. Kim, H. Jeong, S.-B. Leigh, and C.-Y. Jang, "Thermal management of led lighting integrated with hvac systems in office buildings," *Energy and Buildings*, vol. 127, pp. 1159 – 1170, Sep. 2016.

[18] B. Ahn, C. Jang, S. Leigh, S. Yoo, and H. Jeong, "Effect of led lighting on the cooling and heating loads in office buildings," *Applied Energy*, vol. 113, pp. 1484 – 1489, Jan. 2014.

[19] ASHRAE, *ASHRAE Handbook: Fundamentals*, Std., 2001.

[20] U.S. Department of Energy. (2017, Oct.) Energyplus. [Online]. Available: https://energyplus.net/

[21] J. Silvente, G. M. Kopanos, E. N. Pistikopoulos, and A. Espuña, "A rolling horizon optimization framework for the simultaneous energy supply and demand planning in microgrids," *Applied Energy*, vol. 155, no. 1, pp. 485 – 501, Oct. 2015.

[22] F. Oldewurtel, A. Parisio, C. N. Jones, D. Gyalistras, M. Gwerder, V. Stauch, B. Lehmann, and M. Morari, "Use of model predictive control and weather forecasts for energy efficient building climate control," *Energy and Buildings*, vol. 45, pp. 15 – 27, Feb. 2012.

[23] S. Hanif, H. B. Gooi, T. Massier, T. Hamacher, and T. Reindl, "Distributed congestion management of distribution grids under robust flexible buildings operations," *IEEE Trans. Power Syst.*, vol. 32, no. 6, pp. 4600–4613, Nov. 2017.

[24] H. Wang, K. Meng, Z. Y. Dong, Z. Xu, F. Luo, and K. P. Wong, "Efficient real-time residential energy management through MILP based rolling horizon optimization," in *2015 IEEE Power Energy Society General Meeting*, Jul. 2015, pp. 1–6.

[25] R. Palma-Behnke, C. Benavides, F. Lanas, B. Severino, L. Reyes, J. Llanos, and D. Sáez, "A microgrid energy management system based on the rolling horizon strategy," *IEEE Transactions on Smart Grid*, vol. 4, no. 2, pp. 996–1006, Jun. 2013.

[26] J. A. Pinzon, P. P. Vergara, L. C. P. da Silva, and M. J. Rider, "An MILP model for optimal management of energy consumption and comfort in smart buildings," in *2017 IEEE Power Energy Society Innovative Smart Grid Technologies Conference (ISGT)*, April 2017, pp. 1–5.

[27] L. H. Macedo, J. F. Franco, M. J. Rider, and R. Romero, "Optimal operation of distribution networks considering energy storage devices," *IEEE Trans. Smart Grid*, vol. 6, no. 6, pp. 2825–2836, Nov. 2015.

[28] T. Cui, S. Chen, Y. Wang, Q. Zhu, S. Nazarian, and M. Pedram, "Optimal co-scheduling of hvac control and battery management for energy-efficient buildings considering state-of-health degradation," in *2016 21st Asia and South Pacific Design Automation Conference (ASP-DAC)*, Jan. 2016, pp. 775–780.

[29] U.S. Department of Energy, *EnergyPlus Documentation, Engineering Reference-The Reference to EnergyPlus Calculations*, 2015.

[30] N. Wang, F. Fang, and M. Feng, "Multi-objective optimal analysis of comfort and energy management for intelligent buildings," in *The 26th Chinese Control and Decision Conference (2014 CCDC)*, May 2014, pp. 2783–2788.

[31] N. Kruis, "Reconciling differences between residential dx cooling models in doe-2 and energyplus," *Proceedings of SimBuild*, vol. 4, no. 1, pp. 134–141, 2010. [Online]. Available: http://ibpsa-usa.org/index.php/ibpusa/article/view/281

[32] J. F. Franco, M. J. Rider, M. Lavorato, and R. Romero, "Optimal conductor size selection and reconductoring in radial distribution systems using a mixed-integer lp approach," *IEEE Transactions on Power Systems*, vol. 28, no. 1, pp. 10–20, Feb. 2013.

[33] S. Hanif, T. Massier, T. Hamacher, and T. Reindl, "Evaluating demand response in the presence of solar pv: Distribution grid perspective," in *2016 IEEE Smart Energy Grid Engineering (SEGE)*, Aug. 2016, pp. 392–397.

[34] H. Yuan, F. Li, Y. Wei, and J. Zhu, "Novel linearized power flow and linearized OPF models for active distribution networks with application in distribution lmp," *IEEE Transactions on Smart Grid*, vol. 9, no. 1, pp. 438–448, Jan. 2018.

[35] A. Tabares, J. F. Franco, M. Lavorato, and M. J. Rider, "Multistage long-term expansion planning of electrical distribution systems considering multiple alternatives," *IEEE Transactions on Power Systems*, vol. 31, no. 3, pp. 1900–1914, May 2016.

[36] D. Schachinger, S. Gaida, and W. Kastner, "Smart grid communication at the interface of customer buildings with focus on demand response," in *2015 International Symposium on Smart Electric Distribution Systems and Technologies (EDST)*, Sep. 2015, pp. 368–373.

[37] N. Kumar, A. V. Vasilakos, and J. J. P. C. Rodrigues, "A multi-tenant cloud-based dc nano grid for self-sustained smart buildings in smart cities," *IEEE Commun. Mag.*, vol. 55, no. 3, pp. 14–21, Mar. 2017.

[38] J. A. Pinzon, "Optimal management of energy consumption and comfort for smart buildings connected to a microgrid," Master's thesis, Faculty of Electrical and Computer Engineering, Campinas Univ., Campinas, Brazil, 2018.

[39] M. d. C. Tome, "Análise do impacto do chuveiro elétrico em redes de distribuição no contexto da tarifa horossazonal, [analysis of the impact of electric shower in distribution networks in the context of an hourly tariff]," Master's thesis, Faculty of Electrical and Computing Engineering, Campinas Univ., Campinas, Brazil, 2016.

[40] U.S. Department of Energy. (2017, Oct.) Weather data by location. [Online]. Available: https://energyplus.net/weather-location/south_america_wmo_region_3/BRA//BRA_SP_Sao.Paulo.837810_INMET

[41] R. Fourer, D. M. Gay, and B. W. Kernighan, *AMPL: A modeling language for mathematical programming*, 2nd ed. Pacific Grove, CA: Brooks/Cole-Thomson Learning, 2003.

[42] *CPLEX Optimization subroutine library guide and reference*, CPLEX division ed., ILOG Inc., Incline Village, NV, 2008.

[43] ANSI/ASHRAE, *Standards 55-1992, Thermal Environmental Conditions for Human Occupancy*, Std., 1992.

[44] J. C. S. Goncalves, N. S. Vianna, and N. C. da Silva Moura, *Iluminação natural e artificial, [Natural and artificial lighting]*, PROCEL EDIFICA, Rio de Janeiro, Aug. 2011.

[45] *Distribution Test System*, Laboratorio de Planejamento de Sistemas de Energia Elétrica (LaPSEE), UNESP, 2017. [Online]. Available: http://www.feis.unesp.br/#!/departamentos/engenharia-eletrica/pesquisas-e-projetos/lapsee/downloads/materiais-de-cursos1193/

[46] J. K. Gruber and M. Prodanovic, "Two-stage optimization for building energy management," *Energy Procedia*, vol. 62, pp. 346 – 354, 2014, 6th International Conference on Sustainability in Energy and Buildings, SEB-14.

Jerson A. Pinzon received the B.Sc. degree in electric engineering from the Universidad Industrial de Santander, Bucaramanga, Colombia, in 2013, and the M.Sc. degree in electrical engineering from the University of Campinas, UNICAMP, Campinas, Brazil, in 2018. His current research interests include energy efficiency systems, power consumption optimization, models and strategies for smart buildings and urban sustainability.

Pedro P. Vergara was born in Barranquilla, Colombia in 1990. He received the B.Sc. degree in electronic engineering from the Universidad Industrial de Santander, Bucaramanga, Colombia, in 2012, and the M.Sc. degree in electrical engineering from University of Campinas, UNICAMP, Campinas, Brazil, in 2015. He is currently working toward the Ph.D. degree in electrical engineering at the University of Campinas and at the University of Southern Denmark, SDU, Denmark, as part of a double degree program between UNICAMP and SDU. His current research interests include development of methodologies for the optimization, planning, and control of electrical distribution systems with high penetration of distributed generation and renewable energy systems.

Luiz C. P. da Silva graduated in electrical engineering in Federal University of Goias, Goias, Brazil, in 1995 and received the M.Sc. and Ph.D. degrees in electrical engineering from the University of Campinas, UNICAMP, Campinas, Brazil, in 1997 and 2001, respectively. From 1999 to 2000, he was visiting Ph.D. student at the University of Alberta, Edmonton, AB, Canada. Currently, he is an Associate Professor at the University of Campinas, UNICAMP, Campinas, Brazil. His research interests are power system transmission and distribution.

This article has been accepted for publication in a future issue of this journal, but has not been fully edited. Content may change prior to final publication. Citation information: DOI 10.1109/TSG.2018.2822276, IEEE Transactions on Smart Grid

Marcos J. Rider (S'97–M'06–SM'16) received the B.Sc. (Hons.) and P.E. degrees from the National University of Engineering, Lima, Peru, in 1999 and 2000, respectively, the M.Sc. degree from the Federal University of Maranhão, Maranhão, Brazil, in 2002; and the Ph.D. degree from the University of Campinas (UNICAMP), Campinas, São Paulo, Brazil, in 2006 - all in electrical engineering.

Currently, he is a Professor in the Department of Systems and Energy at UNICAMP. His areas of research are the development of methodologies for the optimization, planning, and control of electrical power systems, and applications of artificial intelligence in power systems.